AFRL-RV-PS-
TP-2015-0007

TEMPERATURE DEPENDENCE OF THE $OH^- + CH_3I$ REACTION KINETICS. EXPERIMENTAL AND SIMULATION STUDIES AND ATOMIC-LEVEL DYNAMICS (POSTPRINT)

Xie Jing, et al.

25 November 2013

Journal Article

AIR FORCE RESEARCH LABORATORY
Space Vehicles Directorate
3550 Aberdeen Ave SE
AIR FORCE MATERIEL COMMAND
KIRTLAND AIR FORCE BASE, NM 87117-5776

REPORT DOCUMENTATION PAGE

Form Approved
OMB No. 0704-0188

Public reporting burden for this collection of information is estimated to average 1 hour per response, including the time for reviewing instructions, searching existing data sources, gathering and maintaining the data needed, and completing and reviewing this collection of information. Send comments regarding this burden estimate or any other aspect of this collection of information, including suggestions for reducing this burden to Department of Defense, Washington Headquarters Services, Directorate for Information Operations and Reports (0704-0188), 1215 Jefferson Davis Highway, Suite 1204, Arlington, VA 22202-4302. Respondents should be aware that notwithstanding any other provision of law, no person shall be subject to any penalty for failing to comply with a collection of information if it does not display a currently valid OMB control number. **PLEASE DO NOT RETURN YOUR FORM TO THE ABOVE ADDRESS.**

1. REPORT DATE *(DD-MM-YYYY)*
25-11-2013

2. REPORT TYPE
Journal Article

3. DATES COVERED *(From - To)*
01 Jun 2013 – 18 Sep 2013

4. TITLE AND SUBTITLE
Temperature Dependence of the OH^- + CH_3I Reaction Kinetics. Experimental and Simulation Studies and Atomic-Level Dynamics (Postprint)

5a. CONTRACT NUMBER

5b. GRANT NUMBER

5c. PROGRAM ELEMENT NUMBER
61102F

6. AUTHOR(S)
Jing Xie[1], Swapnil C. Kohale[1], William L. Hase[1], Shaun G. Ard, Joshua J. Melko, Nicholas S. Shuman, and Albert A. Viggiano

5d. PROJECT NUMBER
2303

5e. TASK NUMBER
PPM00004294

5f. WORK UNIT NUMBER
EF002012

7. PERFORMING ORGANIZATION NAME(S) AND ADDRESS(ES)

Air Force Research Laboratory
Space Vehicles Directorate
3550 Aberdeen Avenue SE
Kirtland AFB, NM 87117-5776

[1]Department of Chemistry and Biochemistry
Texas Tech University
Lubbock, TX 79409-1061

8. PERFORMING ORGANIZATION REPORT NUMBER
AFRL-RV-PS-TP-2015-0007

9. SPONSORING / MONITORING AGENCY NAME(S) AND ADDRESS(ES)

10. SPONSOR/MONITOR'S ACRONYM(S)
AFRL/RVBXT

11. SPONSOR/MONITOR'S REPORT NUMBER(S)

12. DISTRIBUTION / AVAILABILITY STATEMENT
Approved for public release; distribution unlimited. (377ABW-2013-0778 dtd 16 Sep 2013)

13. SUPPLEMENTARY NOTES
Accepted for publication in The American Chemical Society: 25 November 2013. Government Purpose Rights.

14. ABSTRACT

Direct dynamics simulations and selected ion flow tube (SIFT) experiments were performed to study the kinetics and dynamics of the OH-+ CH3I reaction versus temperature. This work complements previous direct dynamics simulation and molecular beam ion imaging experiments of this reaction versus reaction collision energy (Xie et al. J. Phys. Chem. A 2013, 117, 7162). The simulations and experiments are in quite good agreement. Both identify the S(N)2, OH- + CH3I > CH3OH + I-, and proton transfer, OH-+ CH3I CH2I-+ H2O, reactions as having nearly equal importance. In the experiments, the 5N2 pathway constitutes 0.64 +/- 0.05, 0.56-4-0.05, 0.51 + 0.05, and 0.46 + 0.05 of the total reaction at 210, 300, 400, and 500 K, respectively. For the simulations this fraction is 0.56 + 0.06, 0.55 +/- 0.04, and 0.50 +/- 0.05 at 300, 400, and 500 K, respectively. The experimental total reaction rate constant is (2.3 +/- 0.6) x 10(-9), (1.7 +/- 0.4) X 10(-9), (1.9 +/- 0.5) X 10-9, and (1.8 +/- 0.5) X 10-9 cm(3)s-1 at 210, 300, 400, and 500 K, respectively, which is approximately 25% smaller than the collision capture value. The simulation values for this rate constant are (1.7 +/- 0.2) X 10-9, (1.8 +/- 0.1) x 10-9, and (1.6 + 0.1) X 10(-9) cm(3)s I at 300, 400, and 500 K. From the simulations, direct rebound and stripping mechanisms as well as multiple indirect mechanisms are identified as the atomic-level reaction mechanisms for both the S(N)2 and proton-transfer pathways. For the S(N)2 reaction the direct and indirect mechanisms have nearly equal probabilities; the direct mechanisms are slightly more probable, and direct rebound is more important than direct stripping. For the proton-transfer pathway the indirect mechanisms are more important than the direct mechanisms, and stripping is significantly more important than rebound for the latter. Calculations were performed with the OW quantum number J equal to 0, 3, and 6 to investigate the effect of OH-rotational excitation on the OH- + CH3I reaction dynamics. The overall reaction probability and the probabilities for the S(N)2 and protontransfer pathways have little dependence on J. Possible effects on the atomistic mechanisms were investigated for the S(N)2 pathway and the probability of the direct rebound mechanism increased with J. However, the other atomistic mechanisms were not appreciably affected by J.

15. SUBJECT TERMS
s(n)2 nucleophilic-substitution; correlated molecular calculations; classical trajectory simulations; exchange-correlation functionals; gaussian-basis sets; direct dynamics; symplectic integration; atomistic mechanisms; energy; hydrogen

16. SECURITY CLASSIFICATION OF:			**17. LIMITATION OF ABSTRACT**	**18. NUMBER OF PAGES**	**19a. NAME OF RESPONSIBLE PERSON** Dr. Raymond Bemish
a. REPORT Unclassified	**b. ABSTRACT** Unclassified	**c. THIS PAGE** Unclassified	Unlimited	12	**19b. TELEPHONE NUMBER** *(include area code)*

THE JOURNAL OF
PHYSICAL CHEMISTRY A

Article

pubs.acs.org/JPCA

Temperature Dependence of the OH + CH_3I Reaction Kinetics. Experimental and Simulation Studies and Atomic-Level Dynamics

Jing Xie,[†] Swapnil C. Kohale,[†] William L. Hase,*[,†] Shaun G. Ard,[‡] Joshua J. Melko,[‡] Nicholas S. Shuman,[‡] and Albert A. Viggiano[‡]

[†]Department of Chemistry and Biochemistry, Texas Tech University, Lubbock, Texas 79409 1061, United States

[‡]Air Force Research Laboratory, Space Vehicles Directorate, Kirtland AFB, New Mexico 87117 5776, United States

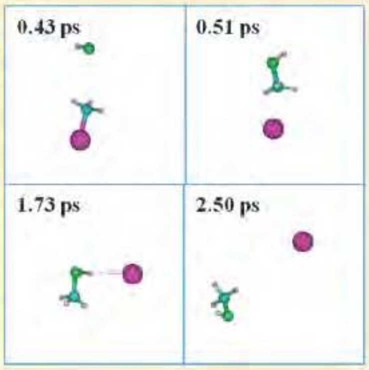

ABSTRACT: Direct dynamics simulations and selected ion flow tube (SIFT) experiments were performed to study the kinetics and dynamics of the OH^- + CH_3I reaction versus temperature. This work complements previous direct dynamics simulation and molecular beam ion imaging experiments of this reaction versus reaction collision energy (Xie et al. *J. Phys. Chem. A* 2013, *117*, 7162). The simulations and experiments are in quite good agreement. Both identify the S_N2, $OH^- + CH_3I \rightarrow CH_3OH + I^-$, and proton transfer, $OH^- + CH_3I \rightarrow CH_2I^- + H_2O$, reactions as having nearly equal importance. In the experiments, the S_N2 pathway constitutes 0.64 ± 0.05, 0.56 ± 0.05, 0.51 ± 0.05, and 0.46 ± 0.05 of the total reaction at 210, 300, 400, and 500 K, respectively. For the simulations this fraction is 0.56 ± 0.06, 0.55 ± 0.04, and 0.50 ± 0.05 at 300, 400, and 500 K, respectively. The experimental total reaction rate constant is $(2.3 \pm 0.6) \times 10^{-9}$, $(1.7 \pm 0.4) \times 10^{-9}$, $(1.9 \pm 0.5) \times 10^{-9}$, and $(1.8 \pm 0.5) \times 10^{-9}$ $cm^3\ s^{-1}$ at 210, 300, 400, and 500 K, respectively, which is approximately 25% smaller than the collision capture value. The simulation values for this rate constant are $(1.7 \pm 0.2) \times 10^{-9}$, $(1.8 \pm 0.1) \times 10^{-9}$, and $(1.6 \pm 0.1) \times 10^{-9}$ $cm^3 s^{-1}$ at 300, 400, and 500 K. From the simulations, direct rebound and stripping mechanisms as well as multiple indirect mechanisms are identified as the atomic level reaction mechanisms for both the S_N2 and proton transfer pathways. For the S_N2 reaction the direct and indirect mechanisms have nearly equal probabilities; the direct mechanisms are slightly more probable, and direct rebound is more important than direct stripping. For the proton transfer pathway the indirect mechanisms are more important than the direct mechanisms, and stripping is significantly more important than rebound for the latter. Calculations were performed with the OH^- quantum number J equal to 0, 3, and 6 to investigate the effect of OH^- rotational excitation on the OH^- + CH_3I reaction dynamics. The overall reaction probability and the probabilities for the S_N2 and proton transfer pathways have little dependence on J. Possible effects on the atomistic mechanisms were investigated for the S_N2 pathway and the probability of the direct rebound mechanism increased with J. However, the other atomistic mechanisms were not appreciably affected by J.

I. INTRODUCTION

Bimolecular reactions of an anion X^- with a methyl halide CH_3Y, e.g., the S_N2 reaction $X^- + CH_3Y \rightarrow CH_3X + Y^-$, are widely studied and are important ion−molecule reactions, particularly in organic chemistry.[1] The dynamics of these reactions have been extensively studied both experimentally[2−4] and computationally.[5−7] During the past few years it has become possible to directly observe the dynamics of ion−molecule reactions by kinematically complete imaging of reactive scattering, which has been applied to charge transfer,[8,9] proton transfer,[13,18] and S_N2 bimolecular nucleophilic substitution reactions.[10−13] These experiments, along with direct dynamics simulations,[6,10,11,13−17] have provided an atomistic understanding of the dynamics of gas phase X^- + CH_3Y reactions.

In recent work,[18] ion imaging and direct dynamics simulations were used to study the atomistic mechanisms for the OH^- + CH_3I reaction at collision energies of 0.05, 0.5, 1.0, 1.5, and 2.0 eV. Direct comparisons between the experiments and simulations were made at 0.5, 1.0, and 2.0 eV, and quite good agreement was found. However, no comparison between experiment and simulation was possible for the lowest collision energy studied in the simulations of 0.05 eV, which is representative of a temperature of ~400 K. We have therefore undertaken a temperature dependent study of the reaction of OH^- with CH_3I from 210 to 500 K, by both experiment and direct dynamics simulations.

The research reported here addresses atomic level mechanisms for the OH^- + CH_3I reaction. The traditional pathway for X^- + CH_3Y reactions is the S_N2 reaction, for which X^- CH_3Y and XCH_3 Y^- pre and postreaction complexes are formed and separated by a central barrier. Both simulation and experiments have shown that X^- + CH_3Y reactions are considerably more rich in detail with additional pathways and numerous atomistic mechanisms, as summarized in Table 1.

Received: September 18, 2013
Revised: November 25, 2013
Published: November 25, 2013

ACS Publications © 2013 American Chemical Society

dx.doi.org/10.1021/jp409347z | *J. Phys. Chem. A* 2013, 117, 14019−14027

Table 1. X^- + CH_3Y S_N2 and Proton Transfer Reaction Mechanisms

Direct	***Rebound:*** X^- attacks the backsides of CH_3Y, directly replacing Y^- for S_N2 (or abstracting an H-atom for proton transfer) reaction, and scattering in the backward direction, with CH_3 inversion for the S_N2 reaction. Tends to be a small impact parameter event; refs 11 and 18.
	Stripping: X^- approaches the side of CH_3Y, stripping off CH_3 for S_N2 (or an H-atom for proton transfer) reaction, and scattering in the forward direction, with CH_3 inversion for the S_N2 reaction. Tends to be a large impact parameter event; refs 11 and 18.
	Front Side Attack: X^- attacks the front side of CH_3Y and directly replaces Y^- without CH_3 inversion; ref 18.
Indirect	***Ion Dipole Complex:*** X^---CH_3Y and XCH_3--Y^- pre- and postreaction complexes; refs 2 and 5.
	Hydrogen-Bonded Complex: X^---HCH_2Y prereaction and CH_3X--Y^- ($X = OH^-$) postreaction complex; refs 11 and 18
	Proton-Transfer Complex: HX--CH_2Y^- ($X = OH^-$); this work. $[CH_3$--Y--$X]^-$ ***Complex;*** refs 18 and 19.
	Roundabout: X^- collides with CH_3Y and the CH_3-group rotates around Y one or more times before S_N2 substitution or proton transfer occurs; ref 10.
	Proton Exchange: $X^- = OH^-$ mechanism for which there is an exchange between the H-atom of OH^- and a H-atom of CH_3Y; ref 18.
	Barrier Recrossing: nonstatistical recrossing of the S_N2 $[X$--CH_3--$Y]^-$ central barrier; refs 14, 20, and 21.

II. COMPUTATIONAL PROCEDURE

The computational procedure used for the simulations was described in detail previously[18] and is briefly summarized here.

A. Electronic Structure Calculations. The NWChem computer program[22,23] was used for the electronic structure calculations. Density functional theory (DFT) calculations,[24] with the B97 1 functional[25] and the ECP/d basis set, give reaction energies in good agreement with experiment.[18] For the ECP/d basis set,[26] Dunning and Woon's aug cc pVDZ basis set[27,28] was used for the H, C, and O atoms. For iodine, the Wadt and Hay effective core potential (ECP)[29] was used for the core electrons and a 3s, 3p basis set for the valence electrons, which was augmented by a d polarization function with a 0.262 exponent and s, p, and d diffuse functions with exponents of 0.034, 0.039, and 0.0873, respectively.

B. Direct Dynamics Simulations. The direct dynamics simulations[30] for the OH^- + CH_3I reaction were performed at the B97 1/ECP/d level of theory. The trajectories for the simulations were calculated using the VENUS chemical dynamics computer program[31,32] interfaced with the NWChem electronic structure computer program.[22,23] To directly compare with the experiments, the simulations were performed for reactant temperatures T of 300, 400, and 500 K. Initial conditions for the trajectories were selected for collision energies (i.e., reagent relative translational energy) of 0.90, 1.05, and 1.20 kcal mol^{-1}, equivalent to $3RT/2$ for the temperatures of 300, 400, and 500 K. Quasiclassical sampling for temperature T was used to select initial conditions for the CH_3I vibrational levels, while the thermal rotational energy of CH_3I was treated classically. Thermal sampling was used to sample the OH^- rotational and vibrational quantum numbers. The OH^- rotational quantum number J was selected according to the distribution $P(J) = (2J + 1) \exp[-J(J + 1)\hbar^2/2Ik_BT]/Q_{rot}$. The vibrational quantum number n was selected from the distribution $P(n) = [\exp(nh\nu/k_BT)]/Q_{vib}$.

In previous simulations,[18] the OH^- + CH_3I reaction was studied at a collision energy of 0.05 eV for fixed OH^- rotational and vibrational quantum numbers $J = 3$ and $n = 0$. The CH_3I rotational and vibrational temperatures were $T_r = 130$ K and $T_v = 330$ K. To study how OH^- rotational energy affects the reaction dynamics, simulations were performed with these initial conditions but with J equal to 0 and 6, to compare with the previous $J = 3$ simulation results.

Semiclassical quantization of the action integral[33] for the potential $[V(r) + J(J + 1)\hbar^2/(2\mu r^2)]$ was performed to select initial conditions for the OH^- n, J vibrational and rotational energy levels. Algorithms for sampling the OH^- + CH_3I initial conditions are standard options in VENUS and have been described previously.[34]

A sixth order symplectic algorithm[35,36] with a 2.5 fs time step was selected to integrate the direct dynamics trajectories. The total integration time for the trajectories was 2.5 ps. Reactive trajectories were identified by viewing animations and thus determining their atomic level mechanisms. The properties determined from the simulations are as follows: reaction pathways and their atomic level mechanisms and reaction cross sections for the different pathways and their individual atomistic mechanisms. The above properties compared with the experiments of Viggiano and co workers are the relative product ion yields and the reaction cross sections and rate constants for the different reaction pathways.

III. EXPERIMENTAL METHOD

The experiments were performed using the Air Force Research Laboratory variable temperature selected ion flow tube (SIFT). The instrument has been well described previously,[37] and only details important to the present measurements are given. OH^- was made in a high pressure ion source through electron impact on H_2O. The OH^- was mass selected using a quadrupole mass filter, injected into the flow tube through a Venturi inlet, and carried downstream by a helium buffer. After typically 3 ms and approximately 10^4 collisions of the OH^- with helium, CH_3I was added through a finger inlet. After a typically 4 ms reaction time, the core of the flow was sampled through a small orifice in a rounded nose cone, while the bulk of the gas was pumped by an oil free Roots type pump. Sampled ions were injected into a quadrupole mass spectrometer and detected using a discrete dynode particle multiplier, operated in ion counting mode.

All flows were measured using MKS mass flow controllers. The ion velocity was calculated from the helium flow velocity and a previously measured ion to helium velocity ratio of ~1.6−1.7. Coupled with the known reaction length of 59 cm, this yields the reaction time. Rate constants were obtained by monitoring the primary decay of OH^- as a function of added neutral concentration in the flow tube as shown in Figure 1a for a 500 K data set. Decays were exponential (linear on the semilog plots shown) over at least 1 order of magnitude. Absolute uncertainties in the rate constants are estimated to be ±25%.[37] Branching ratios were determined by extrapolating plots of percent fraction of each product versus neutral concentration to zero neutral flow as shown in Figure 1b. When the CH_3I concentration was increased, the I^- fraction increased at the expense of CH_2I^-, showing that CH_2I^- reacted with CH_3I to form I^-. At low OH^- depletion the total count rate decreased, while at higher levels of depletion the total counts were constant within about 10%, even though CH_2I^- was being converted into I^-. This behavior indicates that there is some detection discrimination against OH^-, while the discrimination between I^- and CH_2I^- was small. Therefore, we estimate the

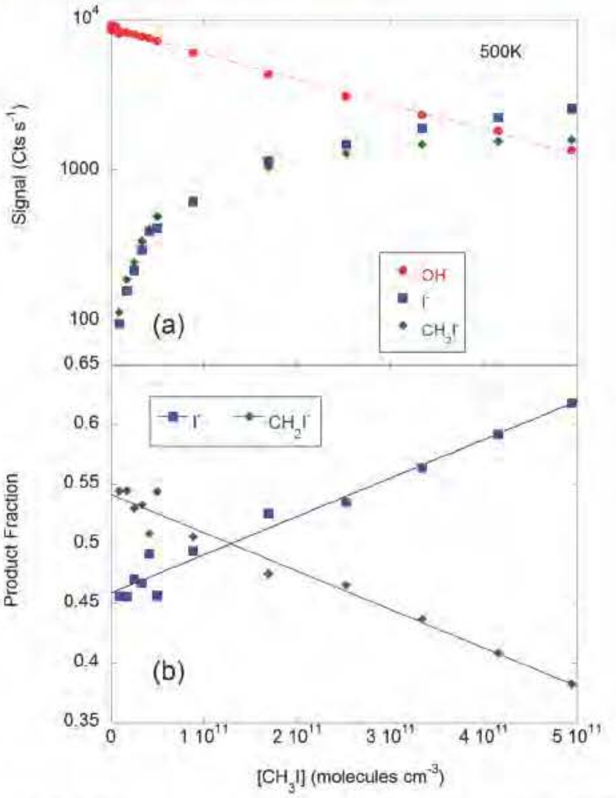

Figure 1. (a) Ion counts as a function of CH_3I concentration at 500 K for the reaction of OH^- with CH_3I, with the best fit line to the primary ion decay shown. (b) Fraction of products as a function of CH_3I concentration; branching fraction values are obtained by extrapolating to a CH_3I concentration of zero.

product fractions to be accurate to about 0.05 absolute (10% discrimination for equal products) and 0.03 relative.

IV. RESULTS AND DISCUSSION

A. Pathways, Anion Product Ratio, and Rate Constants. *1. Simulation Results.* For 300, 400, and 500 K, for which the collision energy is $3RT/2$, a respective total of 311, 385, and 301 trajectories were calculated, and the impact parameter was randomly selected from 0 Å to the maximum impact parameter b_{max} of 9.5, 9.2, and 9.0 Å, respectively. The b_{max} was identified by the impact parameter at which no reaction occurred out of 100 trajectories. The cross section for a reaction pathway σ_r was obtained by multiplying πb^2_{max} by the reaction probability P_r for the pathway. The reaction rate constant k is determined by multiplying the overall total reaction cross section σ_r by the average relative translational velocity $\langle v_{rel} \rangle$.

The following three pathways were observed for each of the three temperatures, and their reaction probabilities are shown in Table 2.

$$OH^- + CH_3I \rightarrow CH_3OH + I^- \quad (1)$$

$$OH^- + CH_3I \rightarrow CH_2I^- + H_2O \quad (2)$$

$$OH^- + CH_3I \rightarrow [CH_3\text{--}I\text{--}OH]^- \quad (3)$$

The overall reaction probability ranges from 0.42 to 0.44, varying very little for the three temperatures. The S_N2 pathway 1 has a higher probability than that for proton transfer 2 at a T of 300 and 400 K, but has a lower probability at 500 K. The probability of the S_N2 pathway is 0.23, 0.23, and 0.20, for 300, 400, and 500 K, respectively. The corresponding probabilities for the proton transfer pathway are 0.18, 0.20, and 0.21. This is the same trend as found in the previous study;[18] i.e., a high collision energy gives more $CH_2I^- + H_2O$, while a low collision energy gives more $CH_3OH + I^-$. As discussed in the previous study,[18] the $[CH_3\ I\ OH]^-$ ion in reaction 3 is an intermediate which has sufficient energy to dissociate if the trajectories were run for a longer period of time. It can either dissociate back to reactants $CH_3I + OH^-$, or react to follow the S_N2 or proton transfer pathways.

2. Comparison between Experiment and Simulation. The three anions I^-, CH_2I^-, and $[CH_3\ I\ OH]^-$ are formed in the simulations and their product ratios, given in Table 3, are obtained directly from the pathway probabilities. Only I^- and CH_2I^- are detected in the experiments, and their ratio is also given in Table 3. Experimentally the I^- yield decreases from 0.64 to 0.46 as the temperature is increased from 210 to 500 K. This trend is also identified from the simulation.

The $[CH_3\ I\ OH]^-$ anion observed in the simulations at the 2.5 ps conclusion of the trajectory integrations will dissociate at longer times. An incomplete study indicates that it dissociates preferentially to the reactants $HO^- + CH_3I$. If it is assumed that all of the dissociation is to $HO^- + CH_3I$, not affecting the relative CH_2I^- to I^- yield, the fraction of the I^- anion in the simulations becomes 0.56, 0.55, and 0.50 at 300, 400, and 500 K, respectively.

The total reaction rate constant is another important property that can be compared between the experiments and simulations. As shown in Table 4, the experimental and simulation rate constants are in quite good agreement. Also given is the collision capture rate constant[38] for each temperature, using the experimental data for the $OH^- + CH_3I$ ion−dipole interaction. The experimental rate constant is approximately 25% smaller than this capture value.

The simulation rate constants are based on the formation of the CH_2I^-, I^-, and $[CH_3\ I\ OH]^-$ anions. The latter species is unstable and, as discussed above, is expected to preferentially dissociate to the $OH^- + CH_3I$ reactants. If it is removed from

Table 2. Temperature Dependence of the Simulation Probabilities for the $OH^- + CH_3I$ Reaction Pathways[a]

	probability			
temperature (K)	total reaction	$CH_3OH + I^-$	$CH_2I^- + H_2O$	$[CH_3\text{–}I\text{–}OH]^-$
300	0.42 ± 0.03	0.23 ± 0.02	0.18 ± 0.02	0.01 ± 0.01
400	0.44 ± 0.03	0.23 ± 0.02	0.20 ± 0.02	0.01 ± 0.01
500	0.43 ± 0.03	0.20 ± 0.02	0.21 ± 0.02	0.02 ± 0.01

[a] The trajectories were terminated at an integration time of 2.5 ps. At longer times all of the $[CH_3\ I\ OH]^-$ anion will dissociate. An incomplete study indicates it will preferentially dissociate to the $CH_3I + OH^-$ reactants.

Table 3. Comparison of the Experiment and Simulation Temperature Dependence of the Anion Product Ratio[a,b]

temperature (K)	CH_2I^-	$[CH_3$--I--$OH]^-$	I^-	I^- (exp)	CH_2I^- (exp)
210				0.64	0.36
300	0.43 ± 0.05	0.03 ± 0.01	0.54 ± 0.06	0.56	0.44
400	0.45 ± 0.04	0.01 ± 0.01	0.54 ± 0.04	0.51	0.49
500	0.48 ± 0.06	0.05 ± 0.01	0.47 ± 0.05	0.46	0.54

[a] See footnote *a* in Table 2 and IV.A.1 Simulation Results concerning the $[CH_3\ \ I\ \ OH]^-$ yield. [b] Experimental branching error estimated to be 0.03 relative and 0.05 absolute.

Table 4. Comparison of the Experiment and Simulation Temperature Dependence of the $OH^- + CH_3I$ Rate Constant[a] and the Calculated Collision Rate Constant

	rate constant (cm^3/s)		
temperature (K)	simulation	exp[b]	calc. coll.[c]
210		2.3×10^{-9}	3.0×10^{-9}
300	1.8 ± 0.1 x10^{-9}	1.7×10^{-9}	2.7×10^{-9}
400	1.8 ± 0.1 x10^{-9}	1.9×10^{-9}	2.5×10^{-9}
500	1.7 ± 0.1 x10^{-9}	1.8×10^{-9}	2.3×10^{-9}

[a] If the $[CH_3\ \ I\ \ OH]^-$ anion is not included in the product yield (see footnote *a* in Table 2), the simulation rate constant becomes 1.7×10^{-9}, 1.8×10^{-9}, and 1.6×10^{-9} cm^3s^{-1} at 300, 400, and 500 K, respectively. [b] Errors in the experimental rate constants are estimated to be ±25%.[37] [c] The collision rate constants are calculated according to ref 38.

the product yield, the simulation rate constant becomes 1.7×10^{-9}, 1.8×10^{-9}, and 1.6×10^{-9} $cm^3\ s^{-1}$ at 300, 400, and 500 K, respectively.

B. Potential Energy Surface for the Proton-Transfer Pathway. To assist in understanding the atomistic mechanisms for the $OH^- + CH_3I \rightarrow H_2O + CH_2I^-$ proton transfer reaction, detailed electronic structure calculations at the B97 1/ECP/d level of theory were performed to investigate the reaction's stationary points, i.e., potential minima and saddle points. Figure 2 presents their structures and relative energies without zero point energy. For comparison, the structures and relative energies of the stationary points for the S_N2 reaction pathway, reported previously at the B97 1/ECP/d level of theory, are also given in Figure 2. For the potential energy profiles for both the proton transfer and S_N2 pathways, the first stationary point in proceeding from the reactants to products is the HO^-–HCH_2I hydrogen bonded prereaction complex. Also shown in Figure 2 is the energy for the $[CH_3\ \ I\ \ OH]^-$ intermediate. With zero point energies included, the reaction energies for both the proton transfer and S_N2 pathways are in quite good agreement with experiment.[18] The B97 1/ECP/d values for these proton transfer and S_N2 reaction energies are −4.2 and −64.9 kcal mol^{-1}(with zero point correction energy included), while the 0 K experimental energies of reaction are −3.1 ± 1.8 and −66.4 kcal mol^{-1}.[18]

As shown in Figure 2, these DFT calculations for the proton transfer pathway predict the existence of a hydrogen bonded prereaction complex $HO^-\ \ HCH_2I$ (A) and a transition state $[HO\ \ H\ \ CH_2I]^-$ (TS1) connecting this complex with the postreaction complex $HOH\ \ CH_2I^-$ (C). In addition, there is a second transition state $[ICH_2\ \ HOH]^-$ (TS2) and a second postreaction complex $CH_2I^-\ \ H_2O$ (D). For the prereaction complex (A), transition state (TS1), and postreaction complex (C), two configurations were found through varying the dihedral angle of H−O−C−I. If we use *cis* and *trans* to describe the structure of each pair, the upper set of energies for A, TS1, and C has H and I in the *trans* position, denoted as A′, TS′, and C′, and the lower set has H and I in a *cis* position, denoted as A″, TS″, and C″. Although the structures are different for each pair, there is only a small difference in their energies. The DFT energy (without ZPE correction) differences are 0.02, 0.14, and 1.22 kcal mol^{-1} for A, TS1, and C, respectively.

The structures for the A, TS1, and C stationary points primarily depend on the distances between the O and C atoms and a H atom as shown in Figure 3. Table 5 gives the r_{OH}, r_{CH}, and r_{CO} distances for the stationary points. As compared to the prereaction complex A, the corresponding postreaction complex C has a shorter OH distance and longer CH and CO distances. The second transition state TS2 and second postreaction complex are found by rotating the H_2O molecule to the hydrogen atom side of the CH_2I group, as compared to the structures for TS1 and C. Both the TS2 and second postreaction complex structures were observed in the trajectory simulations.

C. Probabilities of Atomistic Mechanisms. Reactions 1 and 2 are the most important pathways, and in previous work[18] animations were used to identify and provide detailed descriptions of their atomistic mechanisms at E_{rel} of 0.05, 0.5, 1.0, and 2.0 eV. In the work presented here, the relative importance of the different mechanisms versus temperature is considered.

1. S_N2 Pathway. As observed previously,[18] two direct mechanisms, i.e., rebound and stripping, and several indirect mechanisms were observed for the S_N2 pathway. A direct front side attack mechanism was observed in the previous study at a collision energy of 2.0 eV, but this mechanism was not observed in the current simulations at much lower collision energies. The indirect mechanisms observed in the current study include the roundabout, formation of the $HO^-\ \ HCH_2I$ hydrogen bond complex, formation of the $CH_3OH\ \ I^-$ post reaction complex, central barrier recrossing, proton exchange, and couplings of these events.

Overall, the indirect mechanisms are less important than the direct mechanisms. At 300, 400, and 500 K, the fraction of the indirect mechanisms is 0.47, 0.44, and 0.41, respectively. The corresponding respective fractions for direct rebound and stripping mechanisms are 0.37, 0.34, 0.36, and 0.16, 0.21, 0.23, clearly showing direct rebound to be more important than direct stripping. These fractions are summarized in Table 6.

Figure 4 shows the distribution of the indirect mechanisms. The dominant indirect mechanism involves formation of the $HO^-\ \ HCH_2I$ complex. Proton exchange is the second most important indirect mechanism, and this mechanism is always coupled with formation of the $HO^-\ \ HCH_2I$ complex.

A quite small component of the indirect reaction involves transient formation of the $CH_3OH\ \ I^-$ postreaction complex, as seen in Figure 5. The number of such trajectories is 1 out of 311 at 300 K, 3 out of 385 at 400 K, and 2 out of 301 at 500 K.

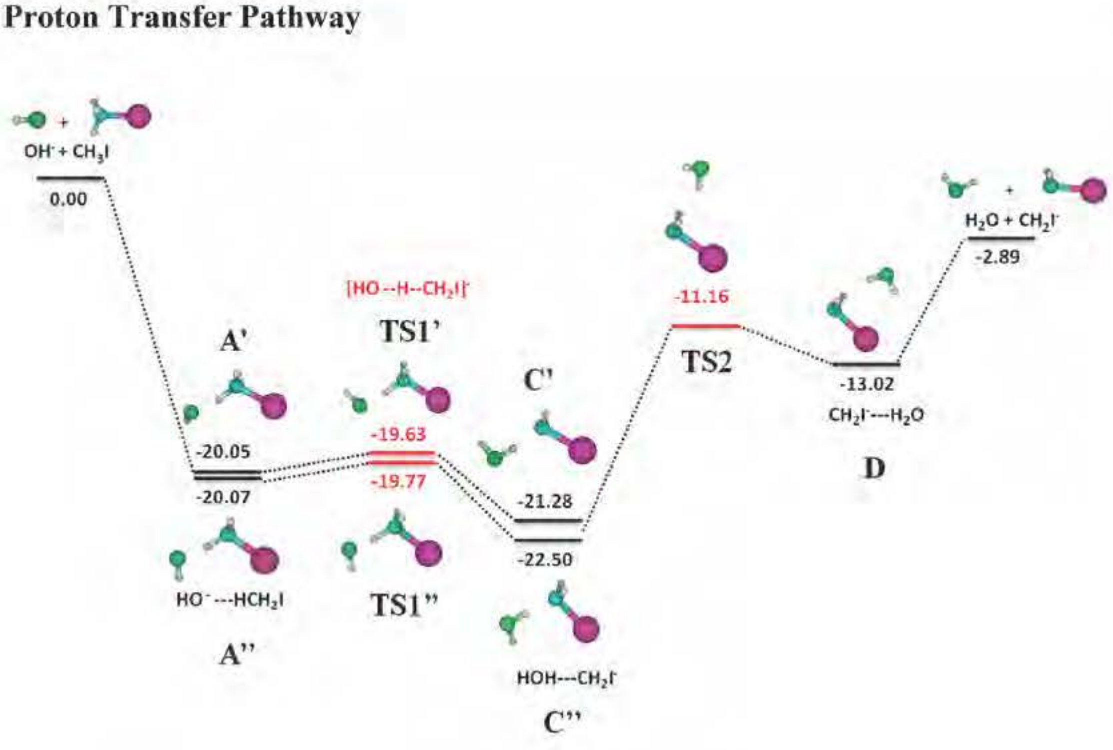
Proton Transfer Pathway
OH⁻ + CH₃I
0.00
A'
-20.05
-20.07
HO⁻---HCH₂I
A"
[HO--H--CH₂I]⁻
TS1'
-19.63
-19.77
TS1"
C'
-21.28
-22.50
HOH---CH₂I⁻
C"
-11.16
TS2
-13.02
CH₂I⁻---H₂O
D
H₂O + CH₂I⁻
-2.89

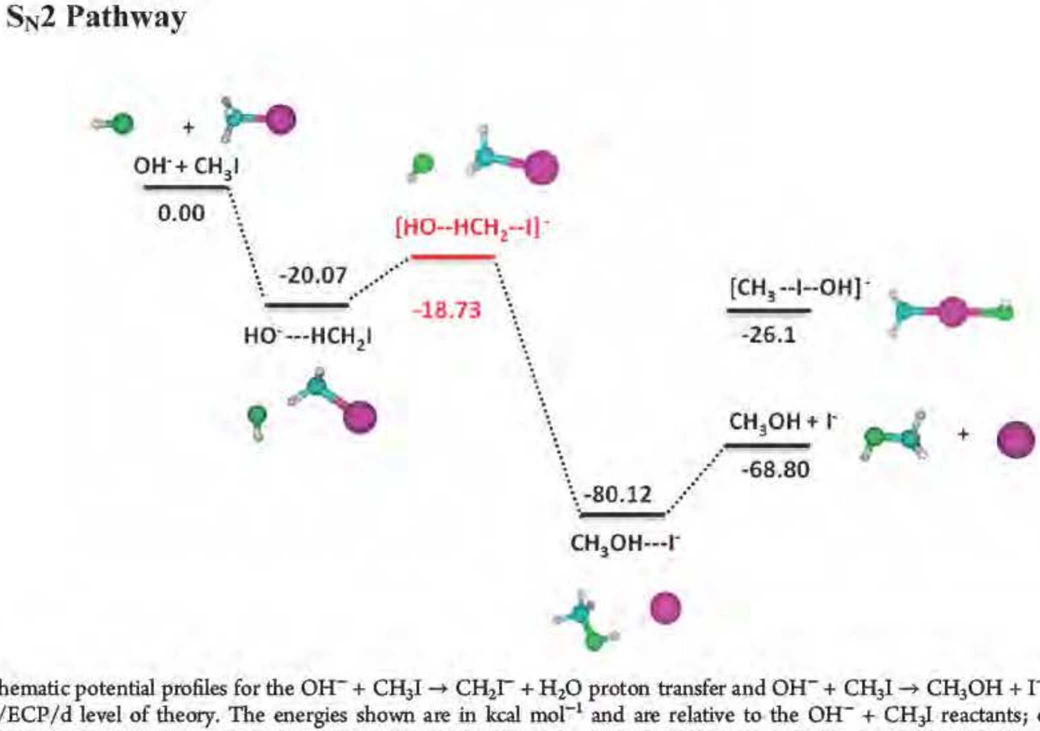
SN2 Pathway
OH⁻ + CH₃I
0.00
-20.07
HO⁻---HCH₂I
[HO--HCH₂--I]⁻
-18.73
-80.12
CH₃OH---I⁻
[CH₃--I--OH]⁻
-26.1
CH₃OH + I⁻
-68.80

Figure 2. Schematic potential profiles for the $OH^- + CH_3I \rightarrow CH_2I^- + H_2O$ proton transfer and $OH^- + CH_3I \rightarrow CH_3OH + I^-$ S_N2 reactions at the DFT/B97 1/ECP/d level of theory. The energies shown are in kcal mol^{-1} and are relative to the $OH^- + CH_3I$ reactants; energies listed in red specify transition state structures. Zero point energies are not included. Two configurations were found for the first transition state and first two intermediates on the proton transfer pathway through varying the dihedral angle of H−O−C−I. If we use *cis* and *trans* to describe the structure of each pair, the upper set of energies for A′, TS1′, and C′ has H and I in the *trans* position, and the lower set, denoted as A″, TS″, and C″, has H and I in a *cis* position.

The CH_3OH I^- complex is a stationary point on the S_N2 pathway. It was not formed in the previous study[18] at much higher collision energies of 0.5, 1.0, and 2.0 eV. Though only a very small percentage of the current trajectories shows formation of the transient CH_3OH I^- complex, this study shows that at lower temperatures, i.e., collision energy, this complex may begin to participate in the reaction dynamics. This complex also has a small participation in the $OH^- + CH_3F$ S_N2 reaction.[15]

2. *CH_2I^- pathway.* The proton transfer pathway, i.e., formation of H_2O and CH_2I^- is as important as the S_N2 pathway at 300, 400, and 500 K. As for the S_N2 pathway, this

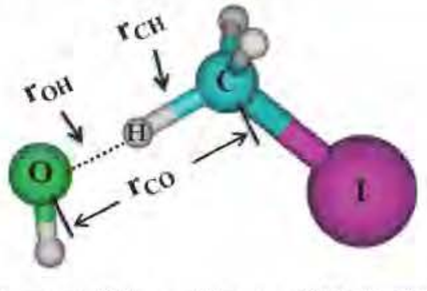

Figure 3. Geometry of the transition state [HO H CH_2I]$^-$ TS1 in Figure 2, which illustrates the distances r_{OH}, r_{CH}, and r_{CO} for Table 5

Table 5. Distances Between O, H, and C Atoms for the Two Sets of Pre reaction Complexes, Transition States, and Post reaction Complexes for the $OH^- + CH_3I \rightarrow CH_2I^- + H_2O$ Proton Transfer Reaction

			distance (Å)[a]		
			r_{OH}	r_{CH}	r_{CO}
upper set	prereaction complex	A′	1.573	1.178	2.728
	transition state	TS1′	1.588	1.174	2.749
	postreaction complex	C′	1.037	1.771	2.804
lower set	prereaction complex	A″	1.553	1.188	2.728
	transition state	TS1″	1.335	1.303	2.632
	postreaction complex	C″	1.033	1.778	2.811

[a] The r's are defined in Figure 3.

Table 6. Simulation Temperature Dependence of the Fractions of the Different Atomistic Reaction Mechanisms for the $OH^- + CH_3I \rightarrow CH_3OH + I^-$ S_N2 and $OH^- + CH_3I \rightarrow CH_2I^- + H_2O$ Proton Transfer Reactions

temperature (K)	DR[a]	DS[a]	IND[a]
		S_N2 reaction	
300	0.37 ± 0.04	0.16 ± 0.05	0.47 ± 0.04
400	0.35 ± 0.04	0.21 ± 0.04	0.44 ± 0.03
500	0.36 ± 0.05	0.23 ± 0.05	0.41 ± 0.04
		proton-transfer reaction	
300	0.06 ± 0.05	0.23 ± 0.05	0.71 ± 0.03
400	0.07 ± 0.04	0.29 ± 0.05	0.64 ± 0.06
500	0.03 ± 0.03	0.32 ± 0.05	0.65 ± 0.03

[a] DR, direct rebound; DS, direct stripping; IND, indirect mechanisms.

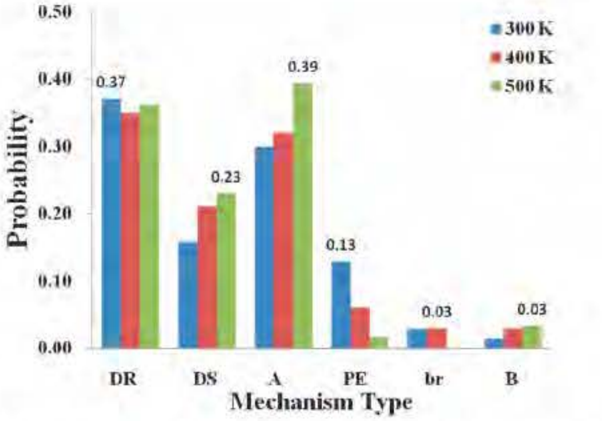

Figure 4. Fractions of the individual atomistic reaction mechanisms for the $OH^- + CH_3I \rightarrow CH_3OH + I^-$ S_N2 reaction at different temperatures: DR, direct rebound; DS, direct stripping; A, HO^- HCH_2I prereaction complex; br, barrier recrossing; PE, proton exchange; and B, CH_3OH I^- postreaction complex.

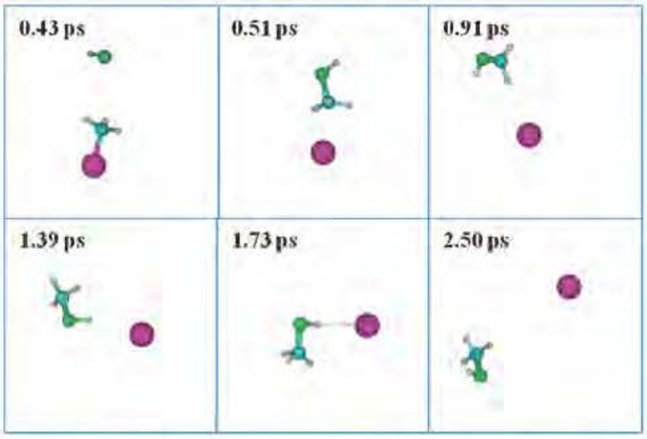

Figure 5. Frames of a sample CH_3OH I^- postreaction complex formation trajectory leading to the $CH_3OH + I^-$ S_N2 products via an indirect mechanism.

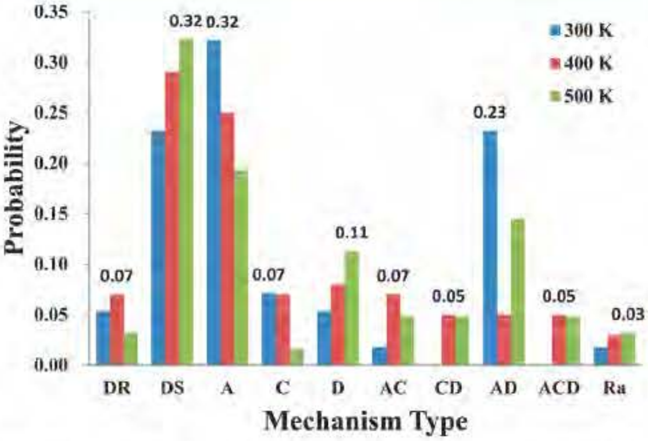

Figure 6. Fractions of the individual atomistic reaction mechanisms for the $OH^- + CH_3I \rightarrow CH_2I^- + H_2O$ proton transfer reaction, at different temperatures: DR, direct rebound; DS, direct stripping; Ra, roundabout; A, HO^- HCH_2I prereaction complex; C, HOH CH_2I^- postreaction complex; and D, CH_2I^- H_2O postreaction complex.

proton transfer pathway occurs via the direct rebound and stripping mechanisms, as well as indirect mechanisms. Table 6 displays the distribution of these mechanisms. The indirect mechanisms dominate, and the fraction ranges from 0.64 to 0.71. Within the two direct mechanisms, direct stripping is more important than direct rebound.

Several types of indirect mechanisms were assigned for the proton transfer pathway. The three stationary point structures on this pathway, observed in the vast majority of the indirect trajectories are the HO^- HCH_2I^-, HOH CH_2I^-, and CH_2I^- H_2O complexes. Identifying HO^- HCH_2I^- as A, HOH CH_2I^-as C, CH_2I^- H_2O as D, roundabout as Ra, the indirect mechanisms are classified as Ra, A, C, D, and the composites of the complexes A+C, C+D, A+D, and A+C+D. The probabilities of these eight indirect mechanisms are shown in Figure 6. In at least 90% of the indirect trajectories, structures were formed for HO^- HCH_2I^- (A) and/or CH_2I^- H_2O (D). It is noteworthy that, though the energy of HOH CH_2I^- (C) is lower than that of CH_2I^- H_2O (D), D is favored before H_2O and CH_2I^- separate. This is because after their formation both CH_2I^- and H_2O have adequate energy to rotate around each other, giving rise to a long lifetime for the CH_2I^- H_2O complex.

Several other relatively unimportant mechanisms occurred for a very few of the trajectories, which are coupled with the above mechanisms. For one of these mechanisms, CH_3OH and I^- were first formed, then associated to form CH_3OH I^-, and through a rearrangement and proton transfer formed CH_2I^- + H_2O. For another, proton transfer occurred twice, and the successful transfer forming products was completed by an H atom from CH_3I different than the one for the first proton transfer. The remaining type is OH^- and CH_3I collision to form $[CH_3\ I\ OH]^-$, which existed for a while before dissociating to CH_2I^- and H_2O.

D. Impact of OH^- Rotational Excitation. Simulations were also performed to study the role of OH^- rotational excitation on the reaction dynamics. The previous simulations[18] at a collision energy of 0.05 eV, with fixed OH^- rotational and vibrational quantum numbers $J = 3$ and $n = 0$, and CH_3I rotational and vibrational temperatures $T_r = 330$ K and $T_v = 130$ K were repeated, but with J equal to 0 and 6. A total of 324, 755, and 325 trajectories were calculated for J of 0, 3, and 6, respectively. The reaction probability, anion product ratios, and mechanisms for the S_N2 pathway were analyzed as a function of J.

As shown in Table 7, the overall reaction probability and the probabilities for the different pathways have at most only a small dependence on J. There is an indication that the overall reaction probability is slightly smaller at $J = 3$, but this is a minor effect. Consequently, the anion product ratio is similar for the three J values. As shown in Table 8, the ratio for I^-: CH_2I^-: $[CH_3\ I\ OH]^-$ is 0.56:0.38:0.06, 0.57:0.37:0.06, and 0.59:0.35:0.06 for J of 0, 3, and 6, respectively. With $[CH_3\ I\ OH]^-$ not included as a product (see IV.A.1 Simulation Results), the respective rate constants are $2.2 \pm 0.2 \times 10^{-9}$, $1.9 \pm 0.1 \times 10^{-9}$, and $2.1 \pm 0.1 \times 10^{-9}$ $cm^3\ s^{-1}$ for J of 0, 3, and 6, respectively. In summary, these simulations indicate that change of the OH^- rotational quantum number does not have a significant effect on the probability of the overall reaction, nor for the different pathways.

Table 7. Simulation Probabilities for the OH^- + CH_3I Reaction Pathways versus OH^- Rotational Quantum Number

	probability			
J (OH^-)	total reaction	$CH_3OH + I^-$	$CH_2I^- + H_2O$	$[CH_3\text{–}I\text{–}OH]^-$
0	0.58 ± 0.03	0.33 ± 0.03	0.22 ± 0.02	0.03 ± 0.01
3	0.49 ± 0.02	0.28 ± 0.02	0.18 ± 0.01	0.03 ± 0.01
6	0.56 ± 0.03	0.33 ± 0.03	0.20 ± 0.02	0.03 ± 0.01

Table 8. Simulation Anion Product Ratios versus the OH^- Rotational Quantum Number

J (OH^-)	CH_2I^-	$[CH_3\text{--}I\text{--}OH]^-$	I^-
0	0.38 ± 0.04	0.06 ± 0.01	0.56 ± 0.05
3	0.37 ± 0.06	0.06 ± 0.01	0.57 ± 0.06
6	0.35 ± 0.04	0.06 ± 0.01	0.59 ± 0.05

A detailed analysis of the dynamics for the S_N2 pathway shows that the value of the OH^- rotational quantum number does influence the atomic level mechanisms. As for the results presented above versus temperature, the direct rebound and stripping mechanisms are dominant. However, as J is increased, the fraction of the direct mechanisms increases and the corresponding fraction of the indirect mechanisms decreases as 0.43 ± 0.06, 0.39 ± 0.05, and 0.36 ± 0.06 for J of 0, 3, and 6, respectively. The fractions for the indirect and direct mechanisms are summarized in Table 9.

Table 9. Simulation Fractions of the Different Atomistic Reaction Mechanisms for the $OH^- + CH_3I \rightarrow CH_3OH + I^-$ S_N2 Reactions versus OH^- Rotational Quantum Number

J (OH^-)	DR	DS	IND
0	0.29 ± 0.04	0.27 ± 0.04	0.43 ± 0.06
3	0.33 ± 0.06	0.28 ± 0.05	0.39 ± 0.05
6	0.39 ± 0.06	0.25 ± 0.04	0.36 ± 0.06

[a] DR, direct rebound; DS, direct stripping; IND, indirect mechanisms.

Although the overall trend is for the direct S_N2 mechanisms to increase with increase in J, this is not the case for the individual direct mechanisms. The probability of the direct rebound mechanism increases with increasing J, while the probability of the direct stripping mechanism remains the same with change in J. The increased fraction of the direct mechanisms with increase in J is contributed to the direct rebound mechanism.

The probabilities of the different indirect S_N2 mechanisms are not affected by J. As shown in Figure 7, formation of the HO^- HCH_2I complex is the dominant mechanism. The proton transfer mechanism is second, followed by barrier recrossing, postreaction complex formation, and roundabout as lesser important mechanisms. In summary, the value of J affects the overall distribution of indirect and direct mechanisms but not the individual indirect S_N2 mechanisms.

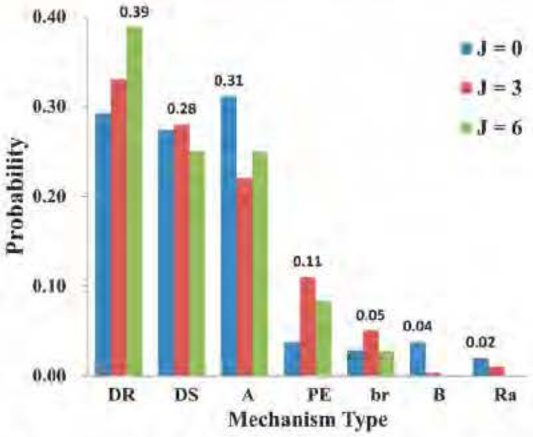

Figure 7. Fractions of the individual atomistic reaction mechanisms for the $OH^- + CH_3I \rightarrow CH_3OH + I^-$ S_N2 reaction versus the OH^- rotational quantum number: DR, direct rebound; DS, direct stripping; Ra, roundabout; A, HO^- HCH_2I prereaction complex; br, barrier recrossing; PE, proton exchange; and B, CH_3OH I^- postreaction complex.

V. CONCLUSION

Both experiments and simulations find that the OH^- + CH_3I reaction for temperatures between 300 and 500 K occur via a S_N2 pathway forming CH_3OH + I^- and a proton transfer pathway forming CH_2I^- + H_2O. The relative importance of these two pathways are similar; the experimental I^- fraction of the anion yield decreases from 0.64 to 0.46 for a temperature change from 210 to 500 K, while the simulation fractional I^- yield decreases as 0.56 ± 0.06, 0.55 ± 0.04, and 0.50 ± 0.05 for the respective temperatures of 300, 400, and 500 K. The reaction intermediate $[CH_3\ I\ OH]^-$ is present in the simulations when the trajectories are ended at 2.5 ps, but this species dissociates primarily to the reactants $CH_3I + OH^-$ at longer times and is not observed in the experiments.

The atomistic mechanisms for the $OH^- + CH_3I$ reaction are at most only weakly affected by the reactant temperature. For the S_N2 pathway, the direct mechanisms are slightly more important than the indirect mechanisms, and rebound is the dominant direct mechanism. The indirect mechanisms are more important than direct mechanisms for the proton transfer pathway, and stripping is the dominant direct mechanism.

Rotational excitation of OH^- does not affect the overall $OH^- + CH_3I$ reaction probability nor the branching between the S_N2 and proton transfer pathways. However, it may affect the probabilities and dynamics of the atomistic mechanisms for these pathways.

■ AUTHOR INFORMATION

Notes

The authors declare no competing financial interest.

■ ACKNOWLEDGMENTS

The direct chemical dynamics simulations reported here are based upon work supported by the National Science Foundation under Grant CHE 0957521 and the Robert A. Welch Foundation under Grant D 0005. Support was also provided by the High Performance Computing Center (HPCC) at Texas Tech University, under the direction of Philip W. Smith and the Texas Advanced Computing Center (TACC) at the University of Texas at Austin. Concerning the experimental work, N.S.S. and A.A.V. are grateful for the support of the Air Force Office of Scientific Research under Project AFOSR 2303EP, while J.J.M. and S.G.A. acknowledge the support of the National Research Council.

■ REFERENCES

(1) Vollhardt, K. P. C.; Schore, N. E. *Organic Chemistry, Structure and Function*; Macmillan: New York, 2003.

(2) Farneth, W. E.; Brauman, J. I. Dynamics of Proton Transfer Involving Delocalized Negative Ions in the Gas Phase. *J. Am. Chem. Soc.* **1976**, *98*, 7891−7898.

(3) Chabinyc, J. L.; Craig, S. L.; Regan, C. K.; Brauman, J. I. Gas Phase Ionic Reactions: Dynamics and Mechanism of Nucleophilic Displacements. *Science* **1998**, *279*, 1882−1886.

(4) Laerdahl, J. K.; Uggerud, E. Gas Phase Nucleophilic Substitution. *Int. J. Mass Spectrom.* **2002**, *214*, 277−314.

(5) Hase, W. L. Simulations of Gas Phase Chemical Reactions: Applications to S_N2 Nucleophilic Substitution. *Science* **1994**, *266*, 998−1002.

(6) Li, G.; Hase, W. L. Ab Initio Direct Dynamics Trajectory Study of the $Cl^- + CH_3Cl$ S_N2 Reaction at High Reagent Translational Energy. *J. Am. Chem. Soc.* **1999**, *121*, 7124−7129.

(7) Manikandan, P.; Zhang, J.; Hase, W. L. Chemical Dynamics Simulations of $X^- + CH_3Y \rightarrow XCH_3 + Y^-$ Gas Phase S_N2 Nucleophilic Substitution Reactions. Nonstatistical Dynamics and Nontraditional Reaction Mechanisms. *J. Phys. Chem. A* **2012**, *116*, 3061−3080.

(8) Mikosch, J.; Frühling, U.; Trippel, S.; Schwalm, D.; Weidemüller, M.; Wester, R. Velocity Map Imaging of Ion−molecule Reactive Scattering: The $Ar^+ + N_2$ Charge Transfer Reaction. *Phys. Chem. Chem. Phys.* **2006**, *8*, 2990−2999.

(9) Pei, L.; Farrar, J. M. Imaging ion−molecule reactions: Charge Transfer and C N Bond Formation in The $C^+ + NH_3$ System. *J. Chem. Phys.* **2012**, *136*, 204305.

(10) Mikosch, J.; Trippel, S.; Eichhorn, C.; Otto, R.; Lourderaj, U.; Zhang, J. X.; Hase, W. L.; Weidemüller, M.; Wester, R. Imaging Nucleophilic Substitution Dynamics. *Science* **2008**, *319*, 183−186.

(11) Zhang, J.; Mikosch, J.; Trippel, S.; Otto, R.; Weidemueller, M.; Wester, R.; Hase, W. L. $F^- + CH_3I \rightarrow FCH_3 + I^-$ Reaction Dynamics. Nontraditional Atomistic Mechanisms and Formation of a Hydrogen Bonded Complex. *J. Phys. Chem. Lett.* **2010**, *1*, 2747−2752.

(12) Otto, R.; Brox, J.; Stei, M.; Trippel, S.; Best, T.; Wester, R. Single Solvent Molecules can Affect the Dynamics of Substitution Reactions. *Nat. Chem.* **2012**, *4*, 534−538.

(13) Otto, R.; Xie, J.; Brox, J.; Trippel, S.; Stei, M.; Best, T.; Siebert, M. R.; Hase, W. L.; Wester, R. Reaction Dynamics of Temperature Variable Anion Water Clusters Studied with Crossed Beams and by Direct Dynamics. *Faraday Discuss.* **2012**, *157*, 41−57.

(14) Sun, L.; Hase, W. L.; Song, K. Trajectory Studies of S_N2 Nucleophilic Substitution. 8. Central Barrier Dynamics for Gas Phase $Cl^- + CH_3Cl$. *J. Am. Chem. Soc.* **2001**, *123*, 5753−5756.

(15) Sun, L.; Song, K.; Hase, W. L. A S_N2 Reaction That Avoids Its Deep Potential Energy Minimum. *Science* **2002**, *296*, 875−878.

(16) Sun, L.; Chang, E.; Song, K.; Hase, W. L. Transition State Dynamics and a QM/MM Model for the $Cl + C_2H_5Cl$ S_N2 Reaction. *Can. J. Chem.* **2004**, *82*, 891−899.

(17) Cheon, S.; Song, K.; Hase, W. L. Central Barrier Recrossing Dynamics of the $Cl^- + CD_3Cl$ S_N2 Reaction. *J. Molec. Struc.: THEOCHEM* **2006**, *771*, 27−31.

(18) Xie, J.; Sun, R.; Siebert, M. R.; Otto, R.; Wester, R.; Hase, W. L. Direct Dynamics Simulations of the Product Channels and Atomistic Mechanisms for the $OH^- + CH_3I$ Reaction. Comparison with Experiment. *J. Phys. Chem. A* **2013**, *117*, 7162−7178.

(19) Seeley, J. V.; Morris, R. A.; Viggiano, A. A.; Wang, H. B.; Hase, W. L. Temperature Dependence of the Rate Constants and Branching Ratios for the Reactions of $Cl^-(D_2O)_{1-3}$ with CH_3Br and Thermal Dissociation Rates for $Cl^-(CH_3Br)$. *J. Am. Chem. Soc.* **1997**, *119*, 577−584.

(20) Cho, Y. J.; Vande Linde, S. R.; Zhu, L.; Hase, W. L. Trajectory Studies of S_N 2 Nucleophilic Substitution. II. Nonstatistical Central Barrier Recrossing in the Cl^-+CH_3Cl System. *J. Chem. Phys.* **1992**, *96*, 8275−8287.

(21) Wang, H.; Peslherbe, G. H.; Hase, W. L. Trajectory Studies of S_N2 Nucleophilic Substitution. 4. Intramolecular and Unimolecular Dynamics of the $Cl^-\ \ CH_3Br$ and $ClCH_3\ \ Br^-$ Complexes. *J. Am. Chem. Soc.* **1994**, *116*, 9644−9651.

(22) Bylaska, E. J.; de Jong, W. A.; Govind, N.; Kowalski, K.; Straatsma, T. P.; Valiev, M.; Wang, D.; Apra, E.; Windus, T. L.; Hammond, J.; et al. *NWChem, A Computational Chemistry Package for Parallel Computers*, version 5.1; Pacific Northwest National Laboratory: Richland, WA, 2007.

(23) Kendall, R. A.; Apra, E.; Bernholdt, D. E.; Bylaska, E. J.; Dupuis, M.; Fann, G. I.; Harrison, R. J.; Ju, J.; Nichols, J. A.; Nieplocha, J. High Performance Computational Chemistry: An overview of NWChem a Distributed Parallel Application. *Comput. Phys. Commun.* **2000**, *128*, 260−283.

(24) Parr, R. G.; Yang, W. *Density Functional Theory of Atoms and Molecules*; Oxford University Press: New York, 1989.

(25) (a) Becke, A. D. Density Functional Thermochemistry. V. Systematic Optimization of Exchange Correlation Functionals. *J. Chem. Phys.* **1997**, *107*, 8554−8560. (b) Hamprecht, F. A.; Cohen, A. J.; Tozer, D. J.; Handy, N. C. Development and Assessment of New Exchange Correlation Functionals. *J. Chem. Phys.* **1998**, *109*, 6264−6272.

(26) Zhang, J.; Hase, W. L. Electronic Structure Theory Study of the $F^- + CH_3I \rightarrow FCH_3 + I^-$ Potential Energy Surface. *J. Phys. Chem. A* **2010**, *114*, 9635−9643.

(27) Dunning, T. H., Jr. Gaussian Basis Sets for Use in Correlated Molecular Calculations. I. The Atoms Boron through Neon and Hydrogen. *J. Chem. Phys.* **1989**, *90*, 1007−1023.

(28) Woon, D. E.; Dunning, T. H., Jr. Gaussian Basis Sets for Use in Correlated Molecular Calculations. III. The Atoms Aluminum through Argon. *J. Chem. Phys.* **1993**, *98*, 1358−1371.

(29) Wadt, W. R.; Hay, P. J. *Ab initio* Effective Core Potentials for Molecular Calculations. Potentials for Main Group Elements Na to Bi. *J. Chem. Phys.* **1985**, *82*, 284−298.

(30) Sun, L.; Hase, W. L. Born Oppenheimer Direct Dynamics Classical Trajectory Simulations. *Rev. Comput. Chem.* **2003**, *19*, 79−146.

(31) Hase, W. L.; Duchovic, R. J.; Hu, X.; Komornicki, A.; Lim, K. F.; Lu, D. H.; Peslherbe, G. H.; Swamy, S. R.; Vande Linde, S. R.; Varandas, A.; et al. *Quantum Chemistry Program Exchange (QCPE) Bulletin.* **1996**, *16*, 671.

(32) Hu, X.; Hase, W. L.; Pirraglia, T. Vectorization of the General Monte Carlo Classical Trajectory Program VENUS. *J. Comput. Chem.* **1991**, *12*, 1014−1024.

(33) Child, M. S. *Semiclassical Mechanics with Molecular Applications*; Oxford University Press: New York, 1991.

(34) Peslherbe, G. H.; Wang, H.; Hase, W. L. Monte Carlo Sampling for Classical Trajectory Simulations. *Adv. Chem. Phys.* **1999**, *105*, 171−201.

(35) Schlier, C.; Seiter, A. Symplectic Integration of Classical Trajectories: A Case Study. *J. Phys. Chem. A* **1998**, *102*, 9399−9404.

(36) Schlier, C.; Seiter, A. High order Symplectic Integration: An Assessment. *Comput. Phys. Commun.* **2000**, *130*, 176−189.

(37) Viggiano, A. A.; Morris, R. A.; Dale, F.; Paulson, J. F.; Giles, K.; Smith, D.; Su, T. Kinetic Energy, Temperature, and Derived Rotational Temperature Dependences for the Reactions of $Kr^+(^2P_{3/2})$ and Ar+ with HCl. *J. Chem. Phys.* **1990**, *93*, 1149−1157.

(38) Su, T.; Chesnavich, W. J. Parametrization of the Ion−Polar Molecule Collision Rate Constant by Trajectory Calculations. *J. Chem. Phys.* **1982**, *76*, 5183−5185.

DISTRIBUTION LIST

DTIC/OCP 8725 John J. Kingman Rd, Suite 0944 Ft Belvoir, VA 22060-6218	1 cy
AFRL/RVIL Kirtland AFB, NM 87117-5776	2 cys
Official Record Copy AFRL/RVBXT/Dr. Raymond Bemish	1 cy